Acta Cryst. (1999). A**55**, 543–557

On the geometry of a modern imaging diffractometer

W. A. Paciorek,† M. Meyer and G. Chapuis*

Institut de Cristallographie, Université de Lausanne, BSP Dorigny, CH-1015 Lausanne, Switzerland.
E-mail: gervais.chapuis@ic.unil.ch

(*Received 27 July 1998; accepted 16 November 1998*)

Abstract

The geometry of a modern imaging diffractometer is discussed in detail. A method to find all relevant instrument parameters from the control single-crystal measurement data is proposed and the limitations of such a procedure are indicated. Optimization of the instrument parameters by the least-squares method is presented.

1. Introduction

The present generation of modern single-crystal diffractometers is more and more frequently equipped with position-sensitive detectors. The overall instrument design varies and is tailored towards the specific experimental requirements (accuracy, resolution, speed, sensitivity, wavelength range *etc.*). Most of the systems are clearly optimized for macromolecular studies and consist of a greatly simplified goniostat (sometimes with only one degree of rotational freedom) and the largest possible imaging detector optimized for a specific radiation wavelength.

A new kind of design has emerged recently. It is based on a conventional goniometer, usually of κ geometry, but with a compact position-sensitive detector replacing the previously used scintillation point detector. The compact position-sensitive detector is based on a detection scheme where an X-ray-sensitive scintillation layer is applied to a fiber-optic reduction taper which is coupled to a charge-coupled device (CCD) imaging detector. Such a scheme allows an overall compact detector design with X-ray sensitive area of 5000 to 12 000 mm^2.

The four-circle imaging goniometer discussed in this paper has three degrees of rotational freedom for the sample orientation and one degree of freedom for the detector swing. Fig. 1 gives a top and a side view of this type of κ-goniometer with a position-sensitive detector. This orientational flexibility allows the efficient measurement of data sets to high resolution (θ-swing) and to full completeness (crystal orientation).

As on any diffractometer system, the quality of the collected data depends on the mechanic and electronic precision of the hardware and, to the same degree, on the precision of the mathematical model used to extract the data. The presence of a position-sensitive detector increases the complexity of such a model and requires a new type of calibration technique. Part of this calibration is the evaluation of the geometric distortions related to the position-sensitive detector itself. For the discussion in this paper, this type of detector is assumed to be distortion free [see Paciorek *et al.* (1999) and references therein for more details].

The calibration of goniometers with position-sensitive detectors has been treated in various articles (Arndt & Wonacott, 1977; Bricogne, 1986; Diamond, 1990; Kabsch, 1988; Thomas, 1990, 1992; Tucker, 1986; Wilkinson, 1990, and references therein). The cited literature does not provide all necessary expressions for a least-squares optimization of a general goniometer model of the type of instrument described above.

In this paper, an attempt is made to extend a common calibration process known from conventional single-crystal diffractometry to this new type of imaging diffractometer. The problem studied here is to evaluate to what extent a reference crystal measurement can be used to verify or even determine the parameters of the geometrical model of the system.

2. Matrix derivatives

To achieve a concise presentation of the results in all subsequent sections, selected results from matrix analysis are presented here. Although all standard formulae from the matrix algebra are commonly used in the crystallographic literature, this seems not to be the case for the matrix analysis.

Let us consider an arbitrary matrix with elements depending on one or more variables. The first definition is a derivative matrix:

$$\partial_x \mathbf{A} = [\partial_x A_{ij}], \tag{1}$$

where x is a generic name for a variable.

Differentiation of this kind obeys a noncommutative chain rule:

† Present address: Global Phasing Ltd, Sheraton House, Castle Park, Cambridge CB3 0AX, England.

$$\partial_x(\mathbf{AB}) = \partial_x\mathbf{AB} + \mathbf{A}\partial_x\mathbf{B} \tag{2}$$

and other familiar rules of differentiation. The useful relation below extends the familiar inverse function differentiation:

$$\partial_x\mathbf{A}^{-1} = -\mathbf{A}^{-1}\partial_x\mathbf{A}\mathbf{A}^{-1}. \tag{3}$$

It is used both to simplify expressions and to avoid symbolic matrix inversion.

A frequent calculation is the normalization of a vector and the simultaneous calculation of its derivatives. A very useful expression to achieve both is:

$$\partial_x(\mathbf{v}/\|\mathbf{v}\|) = \mathbf{M}\partial_x\mathbf{v}, \tag{4}$$

where the following matrix

$$\mathbf{M} = (\mathbf{I} - \mathbf{v}\mathbf{v}^t/\mathbf{v}^t\mathbf{v})/\|\mathbf{v}\| \tag{5}$$

is calculated once and used to normalize all partial derivatives of the given vector.

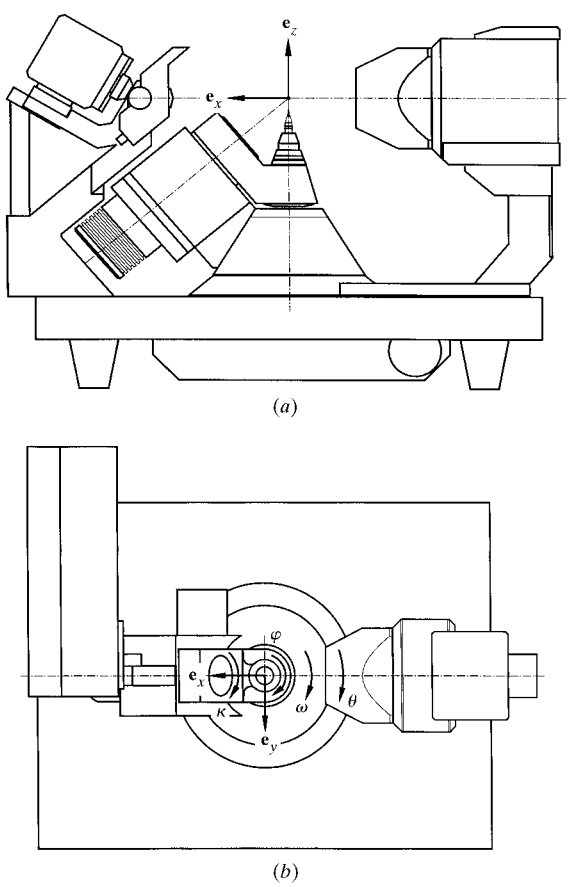

Fig. 1. (*a*) Side and (*b*) top views of the KM4CCD system, a κ goniometer with CCD area detector. The laboratory reference system $\mathbf{e}_x$, $\mathbf{e}_y$, $\mathbf{e}_z$ is indicated: $\mathbf{e}_z$ coincides with the ω-rotation axis, $\mathbf{e}_x$ points in the direction of the X-ray source and $\mathbf{e}_y$ completes the right-handed coordinate system. The positive sense of rotation is given for all instrument axes.

Another useful expression is the differentiation of scalar, vector and matrix functions with respect to variables arranged themselves in vectors. The most common example is

$$\partial_{\mathbf{x}}(\mathbf{Ax}) = \mathbf{A}^t, \tag{6}$$

a special case of which is the differentiation of the scalar product:

$$\partial_{\mathbf{x}}(\mathbf{a}\cdot\mathbf{x}) = \mathbf{a}. \tag{7}$$

A vector product provides an example of another kind of differentiation:

$$\partial_{\mathbf{x}}(\mathbf{a}\times\mathbf{x}) = \mathbf{A}_{\mathbf{a}}, \tag{8}$$

where

$$\mathbf{A}_{\mathbf{a}} = \begin{pmatrix} 0 & -a_z & a_y \\ a_z & 0 & -a_x \\ -a_y & a_x & 0 \end{pmatrix}, \tag{9}$$

where a_x, a_y and a_z are the components of **a**. The result is thus a tensor of higher rank. In this case, it is a skew-symmetric tensor associated with the vector **a** and is an important part of the general rotation operator decomposition. Another important property of the matrix above is

$$\mathbf{A}_{\mathbf{a}}\mathbf{x} = \mathbf{a}\times\mathbf{x}, \tag{10}$$

where **x** is an arbitrary vector.

Some least-squares-optimization problems are formulated and solved by using matrix or vector differentiation. The objective function is a scalar one but parameters are naturally arranged in vectors or matrices.

The first common example of a differentiation with respect to a matrix is

$$\partial_{\mathbf{A}}\det(\mathbf{A}) = \det(\mathbf{A})\,\mathbf{A}^{-1} = \mathrm{adj}(\mathbf{A}), \tag{11}$$

which is frequently used at an intermediate step of formula derivation.

Two important applications used in this paper are the following least-squares residuals:

$$\partial_{\mathbf{x}}\|\mathbf{Ax}-\mathbf{b}\|^2 = 2\mathbf{A}^t(\mathbf{Ax}-\mathbf{b}), \tag{12}$$

$$\partial_{\mathbf{A}}\|\mathbf{Ax}-\mathbf{b}\|^2 = 2(\mathbf{Ax}-\mathbf{b})\mathbf{x}^t, \tag{13}$$

where equation (12) is the familiar linear least-squares problem. Equation (13) occurs when the model parameters are included in the matrix rather than in the vector. Both problems are solved by equating the above equations to zero and solving for a vector or a matrix, respectively.

We conclude this section with a brief account on one of the most useful algorithms of linear algebra, embedded in many computations (like solving linear least-squares problems), the *QR* decomposition.

Every square matrix can be decomposed into a product of two matrices:

$$\mathbf{A} = \mathbf{QR}, \tag{14}$$

where the first is orthogonal:

$$\mathbf{Q}^t = \mathbf{Q}^{-1}, \tag{15}$$

and the second upper triangular:

$$R_{ij} = 0, \quad i > j. \tag{16}$$

In general, this decomposition is not unique. By restricting to nonsingular matrices, one can always find a decomposition with all diagonal elements of the triangular factor positive. The geometrical interpretation of this decomposition will become apparent while discussing properties of the familiar orientation matrix.

Algorithms of the *QR* decomposition can be found in Golub & Van Loan (1996).

3. Orientation matrix

The concept of the orientation matrix is well known and established in single-crystal diffractometry. A brief account is given here as this concept will be used later on not only to handle the geometrical relationship between the reciprocal lattice of the crystal and the diffractometer but also for the geometry of the imaging detector.

The classical definition of the orientation matrix is the product of two matrices (Busing & Levy, 1967):

$$\mathbf{r} = \mathbf{UB}_\lambda \mathbf{h}, \tag{17}$$

where both matrices obey the *QR* decomposition requirement and

$$\mathbf{h} = (h, k, l)^t \tag{18}$$

are the integer Miller indices of a reciprocal-lattice point, considered here as special values of general fractional coordinates. The subscript λ indicates a possible common practice to scale dimensions in the reciprocal space by the wavelength.

The Euclidean length of the vector is

$$\|\mathbf{r}\|^2 = \mathbf{h}^t \mathbf{G}_\lambda \mathbf{h}, \tag{19}$$

revealing the relationship between the orthonormalization matrix and the metric tensor (Prince, 1994):

$$\mathbf{G}_\lambda = \mathbf{B}_\lambda^t \mathbf{B}_\lambda. \tag{20}$$

From the above, it is apparent that this matrix can also be evaluated from the metric tensor alone as its Cholesky factor.

The inverse and transpose of the orthonormalization matrix:

$$\mathbf{L}_\lambda^t = \mathbf{B}_\lambda^{-1} \tag{21}$$

is used to compute the fractional coordinates from the Cartesian ones:

$$\mathbf{h}^t = \mathbf{r}^t \mathbf{UL}_\lambda. \tag{22}$$

In subsequent expressions, we will need simultaneously both of them.

If both kinds of coordinates are known for a large set of points, the optimal orientation matrix can be found by minimizing the least-squares residual:

$$\chi^2 = \sum_n \|\mathbf{UB}_\lambda \mathbf{h}_n - \mathbf{r}_n\|^2, \tag{23}$$

reaching a minimum if the required matrix is

$$\mathbf{UB}_\lambda = \mathbf{RH}^{-1}, \tag{24}$$

where

$$\mathbf{R} = \sum_n \mathbf{r}_n \mathbf{h}_n^t, \tag{25}$$

$$\mathbf{H} = \sum_n \mathbf{h}_n \mathbf{h}_n^t. \tag{26}$$

Equation (13) from the preceding section is used to give an immediate solution.

To facilitate matrix derivative calculations, the orthogonalization matrix can be further decomposed into the following product:

$$\mathbf{B}_\lambda = \mathbf{S}\,\mathrm{diag}(\lambda a^*, \lambda b^*, \lambda c^*), \tag{27}$$

where

$$\mathbf{S} = \begin{pmatrix} 1 & \cos\gamma^* & \cos\beta^* \\ 0 & \sin\gamma^* & -f \\ 0 & 0 & v/\sin\gamma^* \end{pmatrix} \tag{28}$$

is the general shear matrix dependent only on the angular variables.

Its analytical inverse is

$$\mathbf{S}^{-1} = \begin{pmatrix} 1 & -\cot\gamma^* & g/v \\ 0 & 1/\sin\gamma^* & f/v \\ 0 & 0 & \sin\gamma^*/v \end{pmatrix}. \tag{29}$$

Both matrices are defined by three simple trigonometric functions:

$$f = (\cos\beta^* \cos\gamma^* - \cos\alpha^*)/\sin\gamma^*, \tag{30}$$

$$g = (\cos\alpha^* \cos\gamma^* - \cos\beta^*)/\sin\gamma^*, \tag{31}$$

$$v^2/\sin^2\gamma^* = \sin^2\beta^* - f^2 = \sin^2\alpha^* - g^2. \tag{32}$$

From the above equations, all matrix derivatives are easily computed. In the subsequent sections, the above decomposition will be used to handle both the crystal and the detector orientation with respect to the laboratory coordinate system (Wilkinson, 1990).

4. Rotation decomposition

Any rotation can be decomposed into the product of three other rotations around two or three mutually non-parallel axes. The case when two axes suffice is the well known Euler angles representation.

For the refinement of the orientation, it is convenient to represent an arbitrary rotation by a product of

elementary rotations around the given coordinate-system axes. This representation is preferred over the general axis and angle form because it facilitates the refinement of the rotation axis.

Let us consider an arbitrary rotation matrix and derive an algorithm to represent it by the following product:

$$\mathbf{U} = \mathbf{R}_z(\varphi_z)\mathbf{R}_y(\varphi_y)\mathbf{R}_x(\varphi_x), \tag{33}$$

where the elementary rotations are defined as:

$$\mathbf{R}_x = \begin{pmatrix} 1 & 0 & 0 \\ 0 & \cos\varphi_x & \sin\varphi_x \\ 0 & -\sin\varphi_x & \cos\varphi_x \end{pmatrix}, \tag{34}$$

$$\mathbf{R}_y = \begin{pmatrix} \cos\varphi_y & 0 & -\sin\varphi_y \\ 0 & 1 & 0 \\ \sin\varphi_y & 0 & \cos\varphi_y \end{pmatrix}, \tag{35}$$

$$\mathbf{R}_z = \begin{pmatrix} \cos\varphi_z & \sin\varphi_z & 0 \\ -\sin\varphi_z & \cos\varphi_z & 0 \\ 0 & 0 & 1 \end{pmatrix}. \tag{36}$$

Such a decomposition is not unique but this is not important for the problem considered here.

The general solution has already been given in the crystallographic literature and only a brief account and the final results are given here.

The first step is to use the known eigenequation to isolate the inner rotation:

$$\mathbf{e}_z^t\mathbf{U}\mathbf{e}_x = \mathbf{R}_y(\varphi_y), \tag{37}$$

to obtain an equation for the required angle:

$$\varphi_y = \sin^{-1}(U_{31}), \tag{38}$$

which has two possible solutions.

In order to find the other two angles, the degenerate case defined by the following condition:

$$\mathbf{R}_y(\varphi_y)\mathbf{e}_x \neq \pm\mathbf{e}_z \tag{39}$$

has to be checked for. If this condition is satisfied, the final solution reads:

$$\varphi_x = \tan^{-1}(-U_{32}, U_{33}), \tag{40}$$

$$\varphi_z = \tan^{-1}(-U_{21}, U_{11}). \tag{41}$$

Otherwise, one rotation becomes undefined and can be set arbitrarily to zero. The first choice is

$$\varphi_z = \tan^{-1}(U_{12}, U_{22}), \quad \varphi_x = 0, \tag{42}$$

and the second one is

$$\varphi_x = \tan^{-1}(U_{23}, U_{22}), \quad \varphi_z = 0. \tag{43}$$

The method above can be extended to three arbitrary rotations, not necessarily around the coordinate-system axes.

Rotations can also be represented by quaternions of the form (Spena, 1993)

$$q = (\cos(\varphi/2), \mathbf{n}\sin(\varphi/2)), \tag{44}$$

where $\mathbf{n}$ is a unit vector along the rotation axis. Vectors and scalars are represented by quaternions of the special form

$$\mathbf{r} \equiv (0, \mathbf{r}), \quad c \equiv (c, \mathbf{0}). \tag{45}$$

The rotation of a vector is defined as

$$\mathbf{v} = q * \mathbf{r} * q^{-1}. \tag{46}$$

The quaternion representation of rotations has already been used in crystallographic literature for deriving space groups (Bernal, 1923) and to solve an important problem of handling a goniometer with arbitrary geometry (Diamond, 1990).

The following problem, closely related to the κ goniometer, demonstrates a useful property of quaternions as an analytical tool when dealing with general rotations.

Assume that the rotation axis $\mathbf{n}$ is defined by another vector $\mathbf{e}$ rotated by a known rotation, and both are represented by quaternions:

$$q_{\mathbf{m}} = (\cos(\psi/2), \mathbf{m}\sin(\psi/2)) \tag{47}$$

and

$$\mathbf{n} = q_{\mathbf{m}} * \mathbf{e} * q_{\mathbf{m}}^{-1}. \tag{48}$$

Assume that it is desirable to express the former rotation by the new parameters only. Let us compute the following quaternion:

$$q = q_{\mathbf{m}} * q_{\mathbf{m}}^{-1}\cos(\varphi/2) + q_{\mathbf{m}} * \mathbf{e} * q_{\mathbf{m}}^{-1}\sin(\varphi/2). \tag{49}$$

As the scalar multiplication commutes with the quaternion product, it is easy to show that

$$q_{\mathbf{n}} = q_{\mathbf{m}} * q_{\mathbf{e}} * q_{\mathbf{m}}^{-1}, \tag{50}$$

where

$$q_{\mathbf{e}} = (\cos(\varphi/2), \mathbf{e}\sin(\varphi/2)). \tag{51}$$

Thus the former rotation is now represented by a product of three rotations around axes of our choice.

Presenting this result by conventional rotation matrices, we arrive at the equation

$$\mathbf{R}_{\mathbf{n}}(\varphi) = \mathbf{R}_{\mathbf{m}}(\psi)\mathbf{R}_{\mathbf{e}}(\varphi)\mathbf{R}_{\mathbf{m}}^{-1}(\psi), \tag{52}$$

where

$$\mathbf{n} = \mathbf{R}_{\mathbf{m}}(\psi)\mathbf{e}. \tag{53}$$

The above result (or its special case) is frequently used to describe rotations on the κ goniometers, as at least one rotation axis is arbitrary. It is common practice to prefer rotations around laboratory-coordinate-system axes.

Another form of the rotation operator is based on the Cayley–Klein theorem and can be written as

$$\mathbf{R}_\mathbf{n}(\varphi) = \mathbf{P}_\mathbf{n} + \mathbf{A}_\mathbf{n} \sin\varphi - \mathbf{A}_\mathbf{n}^2 \cos\varphi, \tag{54}$$

where

$$\mathbf{P}_\mathbf{n} = \mathbf{P}_\mathbf{n}^2 = \mathbf{n}\mathbf{n}^t \tag{55}$$

is an example of a projection operator. In this form, the rotation angle is clearly separated from the rotation-axis direction and at the same time the three matrices show different symmetry properties.

By using two other properties of the previously introduced skew-symmetric tensor associated with the rotation-axis unit vector:

$$\mathbf{A}_\mathbf{n}^2 = \mathbf{P}_\mathbf{n} - \mathbf{I}, \quad \mathbf{A}_\mathbf{n}^3 = -\mathbf{A}_\mathbf{n}, \tag{56}$$

it is possible to express a rotation entirely by this tensor as follows:

$$\mathbf{R}_\mathbf{n}(\varphi) = \mathbf{I} + \mathbf{A}_\mathbf{n} \sin\varphi + 2\mathbf{A}_\mathbf{n}^2 \sin^2(\varphi/2). \tag{57}$$

This particular form facilitates the derivation of many properties of the rotation operator, like the derivative with respect to the rotation angle:

$$\partial_\varphi \mathbf{R}_\mathbf{n}(\varphi) = \mathbf{A}_\mathbf{n}\mathbf{R}_\mathbf{n}(\varphi), \tag{58}$$

a very useful result to obtain, for example, the derivatives of the diffraction angle.

All the above considerations have been used to develop analytical expressions and algorithms encapsulated in a program module to handle a κ goniometer equipped with a position-sensitive planar detector attached to the same rotating shaft that previously carried a conventional detector. On the diffractometer under consideration, both kinds of detectors can be used.

The coordinate system and some other conventions established previously (like the sense of rotations) have been retained without modification and the only extensions introduced were related to the presence of the imaging detector.

The convention has been adopted that the unit vectors are described by rotations applied to other unit vectors reflecting properties of the so-called perfectly aligned diffractometer, for which these rotations reduce to identities (see Fig. 1 for the choice of the coordinate system).

For example, the primary-beam orientation is given by (Kabsch, 1988)

$$\mathbf{s} = -\mathbf{R}_z(\varphi_z^s)\mathbf{R}_y(\varphi_y^s)\mathbf{e}_x, \tag{59}$$

where the direction is chosen along the momentum carrying vector, leading to the diffraction condition equation (Milch & Minor, 1974), as discussed later in this paper.

A general rotation on the κ goniometer can be written as the following non-commutative product of three rotations:

$$\mathbf{R}_G(\omega, \kappa, \varphi) = \mathbf{R}_\omega \mathbf{R}_\kappa \mathbf{R}_\varphi \tag{60}$$

labelled according to the commonly adopted naming conventions. Fig. 1 indicates the adopted positive sense of rotation. The z axis of the coordinate system coincides with the rotation axis of the ω shaft, but the remaining two shafts are general. For the description of the κ and φ shafts, a simplification is achieved by choosing the x axis in the plane defined by the ω and κ rotation axes. Hence, only one parameter is required to specify the κ shaft. In principle, the remaining φ rotation axis should be given by an arbitrary unit vector (two more parameters). However, by letting another parameter, called the κ offset, be adjusted, an equivalent description can be achieved by adopting a similar form of the rotation matrix for both axes:

$$\mathbf{R}_\psi = \mathbf{R}_y(\alpha_\psi)\mathbf{R}_z(\psi)\mathbf{R}_y(-\alpha_\psi), \quad \psi = \kappa, \varphi. \tag{61}$$

Both of the above rotations are decomposed into products of three elementary rotations around the laboratory-coordinate-system axes and are specified by the actual rotation angle around the z axis and one fixed rotation around the y axis. The fixed rotation angles are the two instrument parameters. Fig. 2 illustrates the instrument parameters α_κ and α_φ with respect to the laboratory coordinate system.

Note that the arrangement described by equation (61) refers to an instrument with arbitrary κ and φ shafts (generalized κ goniometer). An 'ideal' κ goniometer is characterized by $\alpha_\varphi = 0°$, which means that the ω and φ rotation axes coincide at the zero setting of the κ shaft.

The ω and θ rotations are elementary rotations around the z direction:

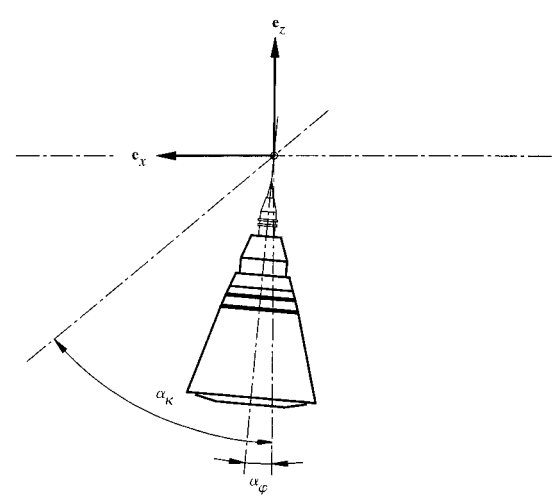

Fig. 2. Illustation of the instrument parameters α_φ and α_κ. For an ideal κ goniometer, these instrument parameters take special values: $\alpha_\varphi = 0°$ and $\alpha_\kappa = 50°$. In this setting, the φ axis coincides with the ω axis at $\kappa = 0°$. These conditions are very difficult to implement on a real instrument. Satisfactory precision of the intersection of the axes can be obtained with relative ease, whereas it is a laborious task to mount the φ axis intersecting with the κ axis at $\alpha_\kappa = 50°$.

$$\mathbf{R}_\psi = \mathbf{R}_z(\psi), \quad \psi = \omega, \theta. \tag{62}$$

The assumption that the detector carrying shaft, θ axis, is parallel to the ω axis reflects the mechanical features of the goniometer. If necessary, it can be replaced by a general one.

The remaining parameters relate the shaft encoder readouts, $\tilde{\psi}$, to the actual angular position. Without lack of generality, these relations can be chosen as simple linear equations:

$$\psi = \tilde{\psi} + \Delta_\psi, \quad \psi = \omega, \kappa, \varphi, \theta, \tag{63}$$

defined for every rotating shaft and included as parameters of the goniometer model to be found. A useful consequence is that all derivatives with respect to the rotation angle are the same as with respect to the corresponding offsets.

5. Diffraction condition

To solve efficiently the diffraction condition equation and simultaneously evaluate all relevant partial derivatives of the diffraction angle, it is convenient to define the following function (Milch & Minor, 1974):

$$f(\varphi) = \mathbf{r}^t\mathbf{r}/2 + \mathbf{s}^t\mathbf{R}(\varphi)\mathbf{r}, \tag{64}$$

where both vectors and the rotation matrix can depend on additional parameters. $\mathbf{r}$ is a reciprocal-space vector [see equation (17)] and $\mathbf{s}$ represents a primary beam as a unit-length vector. The diffraction condition reads:

$$f(\varphi) = 0 \tag{65}$$

and should be solved for the angle. Simultaneously, the above equation defines the diffraction angle as an implicit function of other parameters. Its derivative with respect to any of its parameters is

$$\partial_x\varphi = -\partial_x f/\partial_\varphi f. \tag{66}$$

The denominator is equal to

$$\partial_\varphi f = \mathbf{s}^t\partial_\varphi\mathbf{R}(\varphi)\mathbf{r}. \tag{67}$$

The numerator can take one of the three possible forms as there are no parameters involved simultaneously in all parts of the initial function.

The first derivative involves only parameters of the vector $\mathbf{r}$:

$$\partial_x f = \mathbf{r}^t\partial_x\mathbf{r} + \mathbf{s}^t\mathbf{R}(\varphi)\partial_x\mathbf{r}. \tag{68}$$

The second one involves all rotations:

$$\partial_y f = \mathbf{s}^t\partial_y\mathbf{R}(\varphi)\mathbf{r}, \tag{69}$$

and the last one the primary beam:

$$\partial_z f = \partial_z\mathbf{s}^t\mathbf{R}(\varphi)\mathbf{r}. \tag{70}$$

As the first term in the function f is the square of a vector length, its derivatives with respect of any rotation angles involved in this term vanish.

Assume that the vector $\mathbf{r}$ is given by the rotation of another vector $\mathbf{r}_0$ by some rotation. Not only the length is invariant with respect to this rotation:

$$\|\mathbf{U}(\psi)\mathbf{r}_0\| = \|\mathbf{r}_0\|, \tag{71}$$

but also the following relation holds:

$$\mathbf{r}_0^t\mathbf{U}^t(\psi)\partial_\psi\mathbf{U}(\psi)\mathbf{r}_0 = 0, \tag{72}$$

which greatly simplifies derivative calculations.

To solve the diffraction condition equation, the rotation axis has to be specified. As a first step, the following algorithm has been implemented for solving this condition for elementary rotations.

If the selected rotation is about the z axis, the diffraction condition has the simple form

$$\mathbf{r}^t\mathbf{r}/2 + \mathbf{s}^t\mathbf{R}_z(\varphi)\mathbf{r} = 0 \tag{73}$$

and is solved by the known method of converting a linear trigonometric equation into a quadratic algebraic one. First, the following quantities are computed:

$$\rho = \mathbf{r}^t\mathbf{r}/2 + r_z s_z, \tag{74}$$

$$\varepsilon = r_x s_x + r_y s_y, \tag{75}$$

$$\eta = r_y s_x - r_x s_y. \tag{76}$$

The solution depends on the following discriminant:

$$\Delta = \eta^2 + \varepsilon^2 - \rho^2. \tag{77}$$

If Δ is negative, there is no solution. Otherwise, there are two solutions, possibly degenerate, which are calculated as:

$$\varphi_1 = 2\tan^{-1}(\delta, \rho - \varepsilon), \tag{78}$$

$$\varphi_2 = 2\tan^{-1}(\rho + \varepsilon, \delta), \tag{79}$$

where

$$\delta = -\eta - \mathrm{sgn}(\eta)\Delta^{1/2}. \tag{80}$$

The above equations result from the numerically accurate solution of a quadratic equation (Press *et al.*, 1994).

To accommodate an arbitrary goniometer rotation, the above evaluation can easily be extended. At first, the diffraction condition is recast into the following form:

$$\mathbf{r}^t\mathbf{r}/2 + \mathbf{s}^t\mathbf{R}_G(\varphi)\mathbf{r} = 0. \tag{81}$$

The goniometer rotation is decomposed into the following product:

$$\mathbf{R}_G(\varphi) = \mathbf{R}_s\mathbf{R}(\varphi)\mathbf{R}_r, \tag{82}$$

where the middle rotation is unspecified in angle. If this rotation is about the z axis, the above algorithm is used, but with vectors substituted by:

$$\mathbf{s}^t \leftarrow \mathbf{s}_m^t = \mathbf{s}^t\mathbf{R}_s, \tag{83}$$

$$\mathbf{r} \leftarrow \mathbf{r}_m = \mathbf{R}_r\mathbf{r}. \tag{84}$$

Similar algorithms can be derived for other elementary rotations.

If the crystal orientation matrix is known, the diffraction condition for a given reflection reads:

$$f(\varphi) = \mathbf{h}^t\mathbf{G}_\lambda\mathbf{h}/2 + \mathbf{s}^t\mathbf{R}_G(\varphi)\mathbf{U}\mathbf{B}_\lambda\mathbf{h} \tag{85}$$

and its partial derivatives can be evaluated with respect to some model parameters.

The numerator of the previous generic equations requires only one modification:

$$\partial_\varphi f = \mathbf{s}_m^t\partial_\varphi\mathbf{R}(\varphi)\mathbf{r}_m. \tag{86}$$

The derivatives with respect to the reciprocal-lattice parameters are:

$$\partial_x f = (\mathbf{h}^t\mathbf{B}_\lambda^t + \mathbf{s}^t\mathbf{R}_G\mathbf{U})\partial_x\mathbf{B}_\lambda\mathbf{h}. \tag{87}$$

The derivatives with respect to the crystal and goniometer rotations read:

$$\partial_y f = \mathbf{s}^t\partial_y(\mathbf{R}_G\mathbf{U})\mathbf{B}_\lambda\mathbf{h}. \tag{88}$$

Finally, the derivatives with respect to the primary-beam orientation parameters are:

$$\partial_z f = \partial_z\mathbf{s}^t\mathbf{R}_G\mathbf{U}\mathbf{B}_\lambda\mathbf{h} \tag{89}$$

The above equations provide a valuable part of the least-squares residual. The only missing parameters are those used to describe the detector geometry.

6. Imaging detector

The imaging detector provides as a primary set of observations a large number of images recorded on its surface at given angular settings of the diffractometer. The detector position in space is changing due to the rotation of one of the goniometer axes (detector swing).

In what follows, the detector itself is assumed to be properly calibrated for geometric distortions. The detector is adequately modelled by a plane that may change its orientation in space. The coordinates of a point on this plane can be expressed as a linear combination of three linearly independent vectors defined in the laboratory coordinate system as follows:

$$\mathbf{v} = X\mathbf{d}^X + Y\mathbf{d}^Y - d_0\mathbf{d}^O. \tag{90}$$

The vectors $\mathbf{d}^X$ and $\mathbf{d}^Y$ lie on the detector plane and define a local two-dimensional coordinate system, in which spots have their fractional coordinates X and Y (see Fig. 3).

The vector $\mathbf{d}^O$ links the origin of the detector coordinate system with the laboratory system. The corresponding fractional coordinate d_0 remains fixed for all spots. All three vectors define a new reference frame in space.

The origin-to-origin vector $\mathbf{d}^O$ is usually close to the normal of the detector plane and the degree of this alignment can be easily verified as follows. First the basis vectors in the plane are normalized:

$$\mathbf{n}^I = \mathbf{d}^I/\|\mathbf{d}^I\|, \quad I = X, Y. \tag{91}$$

Then the plane normal vector is evaluated:

$$\mathbf{n} = \mathbf{n}^X \times \mathbf{n}^Y, \tag{92}$$

and finally the required vector is given by the following projection:

$$\mathbf{d}^\perp = \mathbf{n}\mathbf{n}^t\mathbf{d}^O. \tag{93}$$

The length of this vector defines properly the detector distance from the origin of the laboratory system.

The above simple analysis demonstrates that three properly chosen vectors suffice to give a complete description of the planar detector (Thomas, 1990, 1992). The objective is to find them as accurately as possible.

Let us arrange the three vectors in equation (90) as columns of a matrix and perform its QR decomposition:

$$[\mathbf{d}^O, \mathbf{d}^X, \mathbf{d}^Y] = \mathbf{U}_D\mathbf{B}_D. \tag{94}$$

This gives an adequate description of the detector at its zero position. As the detector can be rotated about the diffractometer axis θ, the above matrix should be multiplied by the appropriate rotation matrix:

$$\mathbf{D}_\theta = \mathbf{R}_\theta\mathbf{U}_D\mathbf{B}_D, \tag{95}$$

providing the complete description of the detector plane in an arbitrary position.

The effect of the goniometer rotation on the crystal reciprocal lattice is defined by the following matrix:

$$\mathbf{C}_G = \mathbf{R}_G\mathbf{U}\mathbf{B}_\lambda, \tag{96}$$

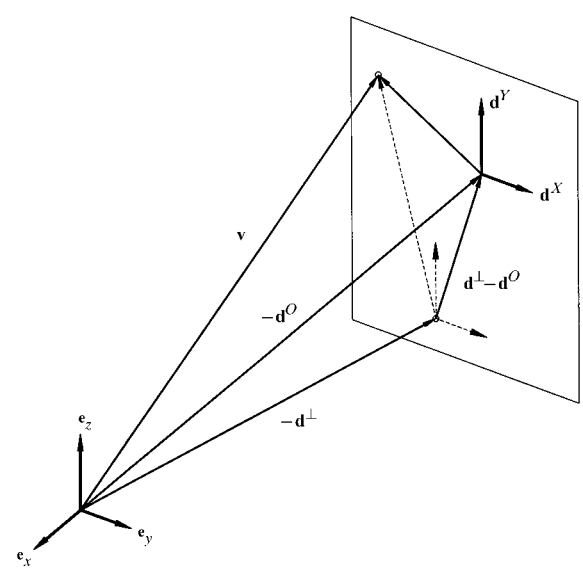

Fig. 3. An ideal position-sensitive detector is adequately modeled by a plane in space. The plane coordinates are expressed in the local two-dimensional coordinate system $\mathbf{d}^X$, $\mathbf{d}^Y$. This system is linked to the laboratory reference system $\mathbf{e}_x$, $\mathbf{e}_y$, $\mathbf{e}_z$ by the origin-to-origin vector $-\mathbf{d}^O$. The plane normal $-\mathbf{d}^\perp$ defines the detector distance from the instrument center.

revealing a close analogy between the crystal and the detector orientation matrices.

Furthermore, let us define the two matrices

$$\widetilde{\mathbf{D}}_\theta = \mathbf{R}_\theta \mathbf{U}_D \mathbf{L}_D, \tag{97}$$

$$\widetilde{\mathbf{C}}_G = \mathbf{R}_G \mathbf{U} \mathbf{L}_\lambda, \tag{98}$$

which are the inverse and transpose of the preceding ones, respectively.

Let us assume that the diffractometer and detector are at a given position and a diffraction spot is recorded. Its two planar coordinates X and Y are given in arbitrary units (usually pixel dimensions). The fractional space coordinates of the spot in the basis defined by equation (90) are

$$\mathbf{p} = (-d_0, X - X_0, Y - Y_0)^t, \tag{99}$$

where an arbitrary origin shift (X_0, Y_0) on the detector plane has been introduced to bring the pixel coordinates close to the detector plane origin. Note that the first coordinate has a different natural length scale than the in-plane coordinates (detector distance *versus* pixel size).

The following unit-length vector is obtained in the laboratory coordinate system:

$$\mathbf{q} = \mathbf{D}_\theta \mathbf{p} / \|\mathbf{B}_D \mathbf{p}\|, \tag{100}$$

in which both the detector position and the detector metric are explicitly included. With the scaling of the reciprocal-space length by the wavelength, this vector is defined on the unit Ewald sphere.

If the diffractometer is positioned at the diffraction condition of the given reflection, the diffracted vector is given by

$$\mathbf{t} = \mathbf{C}_G \mathbf{h} + \mathbf{s}, \tag{101}$$

which is a unit vector on the Ewald sphere. Both above vectors must coincide:

$$\mathbf{C}_G \mathbf{h} + \mathbf{s} = \mathbf{D}_\theta \mathbf{p} / \|\mathbf{B}_D \mathbf{p}\|. \tag{102}$$

This equation provides a relationship between all goniometer, detector and crystal parameters and is the basis for all subsequent analysis.

The following expression is used to extract the Cartesian coordinates of the reciprocal-space points from the recorded spots:

$$\mathbf{r}^t = (\mathbf{q} - \mathbf{s})^t \mathbf{R}_G. \tag{103}$$

At this stage, the crystal orientation matrix is not necessarily known. If it is known, the Miller indices of the reflection can easily be obtained.

The inverse problem is to predict the spot position for a given reflection. The crystal orientation matrix should be known and the diffractometer is assumed to be at the diffraction position.

Let us first compute the following vector:

$$\mathbf{v}^t = \mathbf{t}^t \widetilde{\mathbf{D}}_\theta = \zeta \mathbf{p}, \tag{104}$$

of which the (three) fractional coordinates give the spot position on the detector plane up to an unknown multiplier equal to the inverse of its length.

As the first fractional coordinate is one of the known detector parameters, the above linear system can be easily solved for the unknown spot position coordinates:

$$\zeta = -d_0 / v_1, \tag{105}$$

$$X = \zeta v_2 + X_0, \tag{106}$$

$$Y = \zeta v_3 + Y_0. \tag{107}$$

These equations deserve special attention as they reveal an inherent limitation of any plane-detector-geometry calibration from diffraction data alone. This limitation comes from the fact that the only accessible data are from the projections alone, thus only ratios of dimensions are involved. This is also apparent from equation (102), where the vector normalization is shown explicitly. More details on this will be given later.

Our main objective is to design an optimization algorithm to find the geometrical model parameters. For this purpose, two sets of equations for partial derivatives can be written down and rearranged to emphasize the dependence on the primary beam, the goniometer with the attached crystal and the detector parameters.

As the reference crystal parameters are supposed to be known, the first set of derivatives,

$$\partial_x \mathbf{h}^t = \partial_x \mathbf{q}^t \widetilde{\mathbf{C}}_G, \tag{108}$$

$$\partial_y \mathbf{h}^t = \mathbf{q}^t \partial_y \widetilde{\mathbf{C}}_G, \tag{109}$$

$$\partial_z \mathbf{h}^t = -\partial_z \mathbf{s}^t \widetilde{\mathbf{C}}_G, \tag{110}$$

can be used to reproduce the fundamental crystal lattice property: the integer indexing.

The second set of partial derivatives is used to reproduce the observations themselves, which are mainly the fractional coordinates of the recorded spots. At this stage, the reflection indices are assumed to be known.

Although the spot positions are specified only by two fractional coordinates, the derivatives depend on the three coordinates of the vector defined by equation (90):

$$\partial_x \mathbf{v}^t = \partial_x \mathbf{C}_G \mathbf{h}^t \widetilde{\mathbf{D}}_\theta \tag{111}$$

$$\partial_y \mathbf{v}^t = \mathbf{C}_G \mathbf{h}^t \partial_y \widetilde{\mathbf{D}}_\theta, \tag{112}$$

$$\partial_z \mathbf{v}^t = \partial_z \mathbf{s}^t \widetilde{\mathbf{D}}_\theta. \tag{113}$$

The derivatives of the spot-position coordinates are easily calculated from these expressions.

7. Least-squares residual

The results obtained so far are combined here in a multipart least-squares residual giving the possibility of

optimizing the parameters of different geometrical models from a preferably large set of observations. Each part also has its own weighting scheme.

The first part comes from the difference vectors on the Ewald sphere, defined by equation (102):

$$\chi_E^2 = w_E \sum_n \|\mathbf{w}_n\|^2, \tag{114}$$

where

$$\mathbf{w}_n = \mathbf{C}_G\mathbf{h}_n^o + \mathbf{s} - \mathbf{D}_\theta\mathbf{p}_n^o/\|\mathbf{B}_D\mathbf{p}_n^o\| \tag{115}$$

is the difference between the diffracted vector and the one derived from the observed spot position.

If necessary, a minor modification leads to the alternative difference vector:

$$\mathbf{w}_n' = (\mathbf{C}_G\mathbf{h}_n^o + \mathbf{s})\|\mathbf{B}_D\mathbf{p}_n^o\| - \mathbf{D}_\theta\mathbf{p}_n^o, \tag{116}$$

which is defined on the detector plane.

The next residual aims to reproduce as closely as possible the observed spot positions:

$$\chi_S^2 = w_S \sum_n (\delta X_n^2 + \delta Y_n^2), \tag{117}$$

where

$$\delta X_n = X_n^o - X_n, \quad \delta Y_n = Y_n^o - Y_n \tag{118}$$

are the differences of the observed and calculated fractional coordinates of the spot positions.

The model deficiency can preclude the proper integer indexing of the observed reciprocal-lattice points extracted from the observed spot positions. The model can be improved towards this requirement by minimizing

$$\chi_H^2 = w_H \sum_n \delta\mathbf{h}_n'\delta\mathbf{h}_n, \tag{119}$$

where

$$\delta\mathbf{h}_n = \mathbf{h}_n^o - \mathbf{h}_n \tag{120}$$

and the observed Miller indices are assumed to be known. Finally, all observed spots should be compatible with the diffraction angle condition

$$\chi_D^2 = w_D \sum_n \delta\varphi_n^2, \tag{121}$$

where

$$\delta\varphi_n = \varphi_n^o - \varphi(\mathbf{h}_n^o) \tag{122}$$

is the difference between the observed selected goniometer setting angle and the diffraction angle for a given reflection.

The first residual defined by equation (114) is completely self-contained and reinforces all relevant requirements simultaneously. The others with appropriate weights can be used as penalty functions to force the least-squares optimization to emphasize additional features. The complete residual reads:

Table 1. *Summary of the parameters that may be involved in the most general model describing a κ goniometer with attached imaging detector*

Refer to Figs. 1, 2 and 3 for details of the instrument.

Crystal-related parameters:
(*a*) Crystal orientation (**U**): $\varphi_x^c,\ \varphi_y^c,\ \varphi_z^c$
(*b*) Wavelength-scaled reciprocal-lattice orthonormalization ($\mathbf{B}_\lambda$): $a^*,\ b^*,\ c^*,\ \alpha^*,\ \beta^*,\ \gamma^*$

Goniometer-related parameters:
(*a*) κ-goniometer descriptors ($\mathbf{R}_G$): $\alpha_\kappa,\ \alpha_\varphi$
(*b*) Axis offsets:
(i) Crystal orienter ($\mathbf{R}_G$): $\Delta_\omega,\ \Delta_\kappa,\ \Delta_\varphi$
(ii) Detector orienter ($\mathbf{R}_\theta$): Δ_θ
(*c*) Primary-beam orientation (**s**): $\varphi_y^s,\ \varphi_z^s$

Detector-related parameters:
(*a*) Link between the laboratory reference system and the local two-dimensional coordinate system on the detector plane (origin-to-origin distance) (**p**): d_0
(*b*) Offsets of the detector plane with respect to the 'natural' coordinate system based on the imager pixels grid (assumed to be ideal) (**p**): $X_0,\ Y_0$
(*c*) Detector orientation ($\mathbf{U}_D$): $\varphi_x^d,\ \varphi_y^d,\ \varphi_z^d$
(*d*) Detector orthonormalization ($\mathbf{B}_D$): $a^d, b^d, c^d, \alpha^d, \beta^d, \gamma^d$

$$\chi^2 = \chi_D^2 + \chi_H^2 + \chi_S^2 + \chi_E^2, \tag{123}$$

in which some weights can be set to zero. As all parts never contradict each other, it is perfectly possible to minimize it without restrictions.

The remaining issue is the proper choice of the model parameters and definition of linear constraints, if appropriate. To facilitate this task, let us summarize the complete set of possibly varying parameters and their assignment to the relevant variables:

$$\begin{array}{llllllll}
\mathbf{U} & \varphi_x^c & \varphi_y^c & \varphi_z^c & & & & \\
\mathbf{B}_\lambda & a^* & b^* & c^* & \alpha^* & \beta^* & \gamma^* & \\
 & & & & & & & \\
\mathbf{R}_G & \Delta_\omega & \Delta_\kappa & \Delta_\varphi & \alpha_\kappa & \alpha_\varphi & & \\
\mathbf{s} & \varphi_y^s & \varphi_z^s & & & & & \\
\mathbf{R}_\theta & \Delta_\theta & & & & & & \\
 & & & & & & & \\
\mathbf{p} & d_0 & X_0 & Y_0 & & & & \\
\mathbf{U}_D & \varphi_x^d & \varphi_y^d & \varphi_z^d & & & & \\
\mathbf{B}_D & a^d & b^d & c^d & \alpha^d & \beta^d & \gamma^d. &
\end{array} \tag{124}$$

The complete instrument model is composed of parameter sets describing the reference crystal, the goniometer, the X-ray beam and the detector (see Table 1 for a summary of symbols).

The first set of refined parameters is related to the control crystal. It is assumed that an approximate orientation matrix can be found in advance. The model deficiencies will usually distort the lattice and here a new orientation matrix can be computed by retaining the first (orientation) part but simultaneously overwriting the second and imposing the necessary restrictions on the

refined parameters. For example, in the case of a cubic control crystal, the only refined parameter in $\mathbf{B}_\lambda$ (in addition to the orientation angles) will be the lattice constant a^*. No parameters will be refined in $\mathbf{B}_\lambda$ if the lattice constant of the control crystal is known from another experiment.

The second set of parameters is related to the goniometer axes and the primary beam. In the generalized κ geometry, the goniometer parameters consist of angular offsets Δ_ω, Δ_κ, Δ_φ and Δ_θ for each goniometer shaft and two instrument geometry parameters α_κ and α_φ. The unit vector describing the primary beam requires two additional angular parameters.

Some of these parameters are redundant and have to be fixed on predefined values, usually equal to zero. For example, the φ-axis offset can be fixed, as this is the last rotation axis and it will be absorbed by the crystal orientation matrix.

On this particular instrument, the primary-beam rotation around the z direction is fully correlated with the ω-axis rotation and thus only one of these parameters can be refined.

The offset Δ_θ of the axis rotating the detector plane can be either refined with the corresponding angle φ_z^d of the detector orientation fixed or set to zero while refining the general detector orientation matrix. The third set of parameters is related to the imaging detector. The matrix $\mathbf{U}_D\mathbf{B}_D$ can be controlled in much the same way as for the crystal orientation matrix. Additional precautions are necessary to take properly into account the relative scale of the dimensions involved. In the most general setting, only eight parameters can be refined compared to nine in the case of a crystal (see Tucker, 1986). The parameters involved in the spot-position description are defined by equation (99) and include the origin-to-origin distance d_0 and pixel offsets X_0 and Y_0.

Some representative models will now be discussed in detail.

In the simplest model, the orientation matrix of the detector is a pure rotation. This means that the three vectors $\mathbf{d}_X$, $\mathbf{d}_Y$ and $\mathbf{d}_0$ used to define the detector are orthogonal and $\mathbf{d}_0$ must be normal to the detector plane. The adjustable parameters are the distance d_0 and two offsets X_0 and Y_0 on the detector plane. The complete parameter set, taking into account the parameter redundancy discussed above, is:

$$\begin{array}{llllllll}
\mathbf{R}_G & \Delta_\omega & \Delta_\kappa & 0 & \alpha_\kappa & \alpha_\varphi & & \\
\mathbf{s} & \varphi_y^s & 0 & & & & & \\
\mathbf{R}_\theta & 0 & & & & & & \\
 & & & & & & & \\
\mathbf{p} & d_0 & X_0 & Y_0 & & & & \\
\mathbf{U}_D & \varphi_x^d & \varphi_y^d & \varphi_z^d & & & & \\
\mathbf{B}_D & 1 & 1 & 1 & \pi/2 & \pi/2 & \pi/2. &
\end{array} \tag{125}$$

Based on this model, two further models can be constructed. They differ only in the detector handling part, $\mathbf{p}$, $\mathbf{U}_D$ and $\mathbf{B}_D$, so that the goniometer parameters $\mathbf{R}_G$, $\mathbf{s}$ and $\mathbf{R}_\theta$ are removed from the subsequent summary equations (126) and (127). Note that the following models focus on a subtle difference in describing the detector with respect to the laboratory reference system.

The first model illustrates the relationship between the distance parameter and the pixel size unit. Keeping the origin-to-origin vector length d_0 and the offsets X_0 Y_0 fixed [indicated in summary equation (126) by bars on the respective parameters], one may refine the scale a^d in the orthonormalization matrix and the angular components β^d and γ^d which describe the orientation of the origin-to-origin vector with respect to the local two-dimensional coordinate system. This local coordinate system is assumed to be orthonormal. Evaluating the product $\bar{d}_0 a^d$ gives the distance between the origins but not necessarily measured along the detector plane normal:

$$\begin{array}{llllllll}
\mathbf{p} & \bar{d}_0 & \bar{X}_0 & \bar{Y}_0 & & & & \\
\mathbf{U}_D & \varphi_x^d & \varphi_y^d & \varphi_z^d & & & & \\
\mathbf{B}_D & a^d & 1 & 1 & \pi/2 & \beta^d & \gamma^d. &
\end{array} \tag{126}$$

The last example is used to verify if the local coordinate system on the detector plane is indeed orthogonal. Like in the previous model, the X_0 and Y_0 origins are kept fixed [indicated in summary equation (127) by bars over these entities]. The distance scale a^d is set to one in the orthogonalization matrix, so that the distance is refined directly as d_0. Only one in-plane pixel size (here b^d) is set to one, while the second one and all angles are refined. The model setting is given in the following summary:

$$\begin{array}{llllllll}
\mathbf{p} & d_0 & \bar{X}_0 & \bar{Y}_0 & & & & \\
\mathbf{U}_D & \varphi_x^d & \varphi_y^d & \varphi_z^d & & & & \\
\mathbf{B}_D & 1 & 1 & c^d & \alpha^d & \beta^d & \gamma^d. &
\end{array} \tag{127}$$

The last model is well suited to verify if the geometrical correction of the detector is correct. The c^d parameter being very close to one and α^d being close to the right angle shows that the geometrical correction is appropriate.

8. Tests and results

A least-squares optimization program has been written based on the previously presented results. All derivatives have been carefully tested numerically (Press *et al.*, 1994). A number of simulations have been performed to gain insight on how accurately and under what conditions the method can reproduce the correct geometrical model of the imaging diffractometer.

A reference parameter set was selected to simulate a perfectly aligned system. The parameters chosen represent typical working parameters of the KM4CCD system. This parameter set is shown below:

$$
\begin{array}{lccccccc}
\mathbf{R}_G & 0 & 0 & 0 & 5\pi/18 & 0 & & \\
\mathbf{s} & 0 & 0 & & & & & \\
\mathbf{R}_\theta & 0 & & & & & & \\
 & & & & & & & (128) \\
\mathbf{p} & 1270 & 512 & 512 & & & & \\
\mathbf{U}_D & 0 & 0 & 0 & & & & \\
\mathbf{B}_D & 1 & 1 & 1 & \pi/2 & \pi/2 & \pi/2. &
\end{array}
$$

Synthetic data sets were calculated using a known crystal lattice and orientation. The data sets consisted of the reflection index, spot coordinates and their angular goniometer settings. 950 calculated data were used for the simulations. The least-squares minimization was initiated from a distorted goniometer model using a restricted implementation of the Levenberg–Marquardt method (the damping parameter fixed).

On error-free data sets, the method is capable of exactly reproducing the original model parameters and converges quickly with a large radius of convergence. The crystal orientation and lattice parameters were reproduced correctly. Note that it is advisable to use a cubic reference crystal to limit the orthonormalization matrix $\mathbf{B}_\lambda$ to a single refineable parameter only.

In the next series of tests, random errors of growing amplitude have been added to the spot positions and/or diffraction angles in order to simulate the error of data extraction from actual diffraction images. The refinements have been performed ten times for ten fixed error amplitudes using a system random-number generator. The refinement process showed good convergence with all error amplitudes but the model parameters thus obtained gradually degraded with respect to the known model as the error amplitude increased. The progressive degradation could be observed on all model parameters. The unit-cell parameters of the cubic reference crystal displayed distortions when applying the fitted model to the simulated raw data containing random error. The relation between the error magnitude and the model parameter degradation (measured by the difference between the ideal and fitted parameters) is not fully understood. Fig. 4 gives a graphical representation of the distortions of the lattice parameters a and α for the set of ten error amplitudes and ten random trials each.

After the tests described above, the algorithm was integrated into the diffractometer control software of the KM4CCD system and further tests were conducted on the actual crystal data.

First, ten different data sets were collected using the same cubic reference sample. The data sets were composed of 15 randomly oriented goniometer settings, each one covering a range of 10–20°. For all sets, the model parameters given under summary equation (125) were refined. Table 2 gives a summary of the experiments and the model parameters thus obtained. The model parameters reproduce quite well in the different data sets but some parameter spread is also noticeable. As the 'true' geometrical model of the goniometer is unknown, it is now impossible to give a final model validation. Applying the fitted model to another known sample and recording its lattice parameters cross validates the instrument model. It was found that the model obtained from the reference crystal is transferable to other samples. An example is given in Table 3.

From the experimental findings, we can conclude that the cells obtained from a typical rotation-method data set are less accurate than the data from a well aligned conventional diffractometer. The precision of the cell data extracted from the rotation-method data depends critically on the frame width and the data spanning. Usually, data sets with several goniometer settings improve the cell quality. For typical frame widths of 0.5–2°, the cell deformations do not exceed 0.05° for a well spanned data set. This precision allows Bravais-cell extraction with a high level of confidence.

For the rotation-method data collection, two types of data sets have generally to be distinguished: wide-range scans for intensity extraction and short-range scans for peak-position extraction. The borderline between the two types of acquisition is diffuse. In general, intensities are collected from a few goniometer settings only, the extreme case being a one-axis spindle machine with symmetric detector (typical imaging-plate set-up). These data sets with limited goniometer-setting variation allow only a subset of parameters to be refined. On several data sets, we attempted to improve the current model found from the reference crystal by refining relevant model parameters on the peak data of the crystal under investigation (usually of low symmetry). The refinement may slightly improve the cell parameters, but results from the model thus obtained may lose their transferability.

The origins of the unit-cell deformation, as seen in Fig. 4, are linked to the uncertainty of the assignment of the diffraction angle and spot position. Compared to the scan widths applied during the centering procedure of a conventional diffractometer, the scan widths applied in the rotation method are one or two orders of magnitude bigger (of the order of 0.1–2°). The assignment of the peak maximum within the frame range is arbitrary, leading to an average assignment error of approximately half of the frame width. The same is true for the assignment of the spot position. In our software implementation, the centroid position is used. This position is defined with respect to the maximum of a fixed size extraction window (typically 7×7 pixels). Additionally, area detectors may suffer from systematic geometric distortions due to the readout mechanics (imaging plate), fiber-optic taper deformations (CCD detectors) and electric field irregularities (wire chambers and electron tube area detectors), to name a few. Our experimental system (CCD detector with attached fiber-optic taper) has been calibrated by an optical method described in Paciorek *et al.* (1999), which allows peak-position

reconstruction from the deformed pattern with an error of less than one pixel.

Finally, the refinement method was applied to data sets from the same sample for different wavelengths. The goal of this test was to see whether the goniometer constants α_κ and α_φ, which are wavelength independent, could be reproduced in all data sets. We used the typical crystallographic wavelengths Cu, Mo and Ag. The instrument constants α_φ and α_κ were reproduced within standard uncertainties. Table 4 summarizes the findings.

9. Concluding remarks

This work presents a general geometric model for imaging diffractometers. All the necessary expressions are presented for the optimization by least squares. The

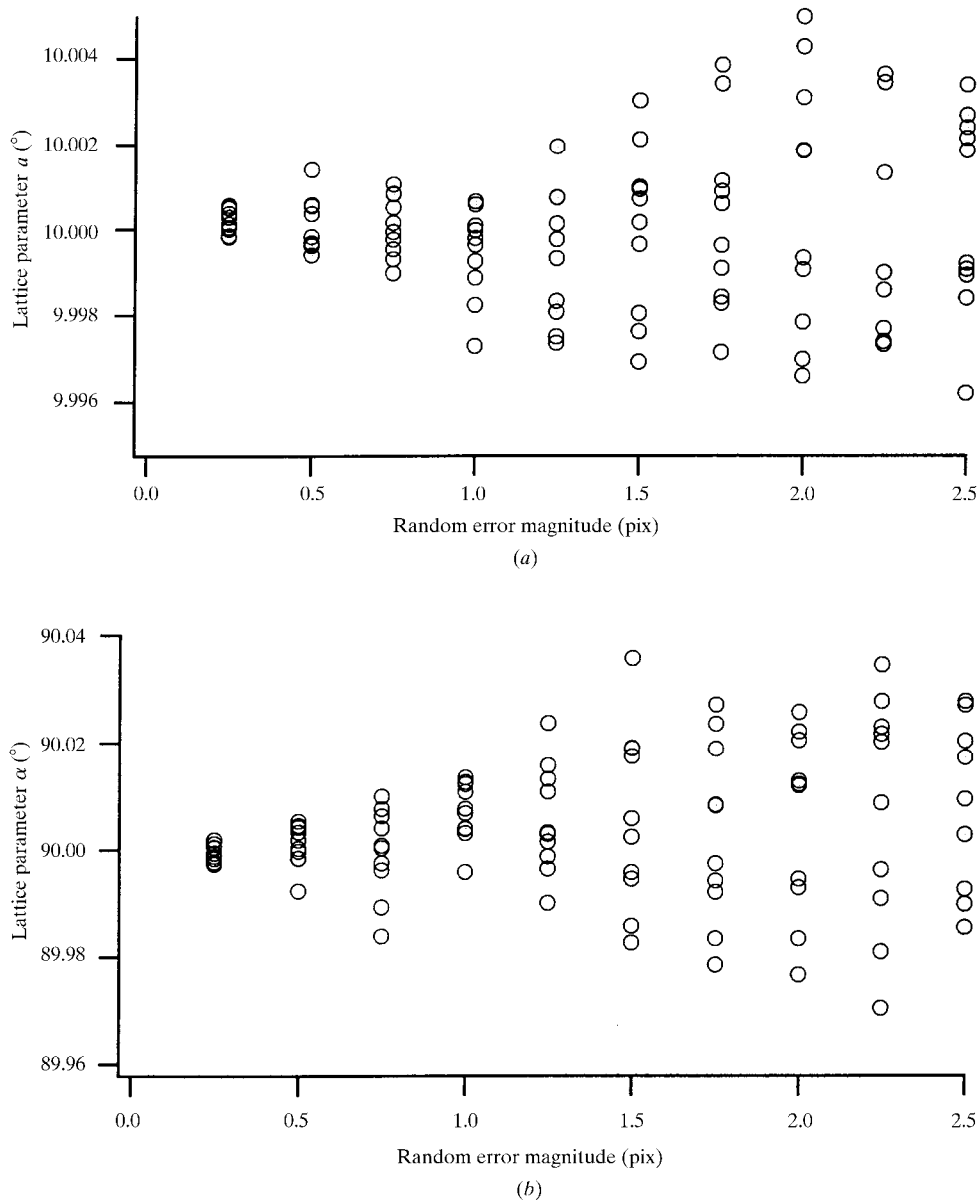

Fig. 4. Distortion of the lattice parameters a and α as a function of random-error magnitude. The plots contain data from 100 synthetic data sets. The spot positions of the ideal reference model [see summary equation (128)] are deteriorated by a zero-mean random error of ten different magnitudes derived from a random-number generator. The magnitudes are scaled to represent the peak extraction uncertainty in the typical 2×2 binning readout mode of the CCD detector on the KM4CCD system. Each data set was then used to find the complete goniometer model [summary equation (128) plus reciprocal-lattice scaling a^* under cubic constraint] by least-squares optimization. The fitted model was used to find the best unconstrained $\mathbf{UB}_\lambda$ from the deteriorated data. The plots show the increasing spead of the lattice distortions in both lattice dimension and cell angles. For typical frame widths of 0.5–2°, the cell-angle deformations do not exceed 0.05° for a well spanned data set.

Table 2. *Calibration of the KM4CCD system using Mo Kα wavelength from randomly composed runs*

All data sets consist of 15 randomly oriented goniometer settings covering a scanning range of 10–20° each, $T^{\rm exp} = 5$ s, $\omega^{\rm step} = 0.5°$. Note that the model refinement was performed under cubic lattice constraint (refined value a^*). The lattice parameters a, b, c, α, β and γ are taken from a constraint-free linear least-squares refinement on the raw reflection data using the previously refined model.

Parameter	1	2	3	4	5	6	7	8	9	10	Average	Standard deviation
$N^{\rm obs}$	935	958	963	959	962	807	971	927	941	999		
χ^2	0.00986	0.009668	0.008974	0.00884	0.008969	0.010086	0.00966	0.009621	0.009597	0.009605		
$\Delta\omega$	0.053	0.036	0.053	0.056	0.056	0.040	0.049	0.060	0.055	0.054	0.051	0.007
$\Delta\kappa$	0.00	0.02	0.00	0.00	0.00	0.03	0.01	−0.01	0.00	0.01	0.01	0.01
α_κ	50.119	50.092	50.106	50.106	50.118	50.101	50.090	50.130	50.113	50.10761	50.108	0.012
α_φ	−0.159	−0.175	−0.164	−0.173	−0.162	−0.171	−0.183	−0.150	−0.167	−0.172	−0.168	0.009
Δ_ϑ	−0.214	−0.204	−0.237	−0.242	−0.219	−0.245	−0.215	−0.220	−0.196	−0.200	−0.219	0.017
d_0	65.020	65.021	65.020	65.021	65.018	65.030	65.028	65.021	65.019	65.016	65.021	0.004
X_0	501.8	502.0	501.4	501.2	501.7	501.2	501.8	501.7	502.2	502.1	501.7	0.3
Y_0	519.7	519.1	518.6	519.0	519.4	518.4	519.4	519.9	519.3	519.7	519.2	0.5
φ_x^d	−0.39	−0.40	−0.39	−0.38	−0.39	−0.40	−0.39	−0.39	−0.39	−0.39	−0.39	0.01
φ_y^d	−0.06	−0.05	−0.01	−0.03	−0.05	−0.02	−0.07	−0.06	−0.05	−0.07	−0.05	0.02
φ_y^s	0.01	−0.02	0.00	0.00	0.00	−0.02	−0.02	0.02	0.00	0.00	0.00	0.01
φ_x^c	98.40	98.39	98.41	98.40	98.41	98.40	98.40	98.43	98.41	98.39	98.40	0.01
φ_y^c	38.84	38.86	38.84	38.85	38.84	38.85	38.86	38.82	38.84	38.84	38.84	0.01
φ_z^c	−166.07	−166.06	−166.07	−166.07	−166.08	−166.07	−166.08	−166.09	−166.08	−166.07	−166.07	0.01
a^*	0.082210	0.082216	0.082214	0.082210	0.082209	0.082206	0.082206	0.082208	0.082210	0.082213	0.082210	0.000003
a (Å)	12.163 (1)	12.164 (1)	12.162 (1)	12.163 (1)	12.163 (1)	12.164 (2)	12.164 (1)	12.163 (1)	12.164 (1)	12.161 (1)		
b (Å)	12.162 (1)	12.161 (1)	12.162 (1)	12.163 (1)	12.162 (1)	12.161 (2)	12.161 (1)	12.164 (1)	12.162 (1)	12.163 (1)		
c (Å)	12.163 (1)	12.163 (1)	12.164 (1)	12.164 (1)	12.165 (1)	12.166 (2)	12.166 (1)	12.162 (1)	12.163 (1)	12.163 (1)		
α (°)	90.027 (9)	90.016 (9)	90.020 (9)	90.024 (9)	90.016 (9)	90.01 (1)	90.021 (9)	90.035 (9)	90.036 (9)	90.042 (9)		
β (°)	89.956 (9)	89.970 (9)	89.977 (9)	89.972 (9)	89.964 (9)	89.98 (1)	89.959 (9)	89.961 (9)	89.953 (9)	89.952 (9)		
γ (°)	90.025 (9)	90.033 (9)	90.035 (9)	90.036 (9)	90.032 (9)	90.05 (1)	90.025 (9)	90.034 (9)	90.022 (9)	90.020 (9)		
V (Å^3)	1799.21	1799.17	1799.14	1799.46	1799.51	1799.6	1799.75	1799.45	1799.46	1799.08		

Table 3. *Example of a lattice determination using a calibration model from a cubic reference crystal applied to 'Ylid', 2-dimethylsulfuranylidene-1,3-indanedione (Christensen & Thom, 1971)*

Experimental details: the 650 peak positions are extracted from a complete data collection composed of three goniometer settings covering 110–250° each.

Parameter	Ylid (Mo)
N^{obs}	650
N^{frames}	434
T^{exp} (s)	25
ω^{step} (°)	1.2
a (Å)	5.978 (1)
b (Å)	9.054 (2)
c (Å)	18.425 (3)
α (°)	90.00 (2)
β (°)	89.99 (2)
γ (°)	90.01 (2)
V (Å^3)	997.21

model has been exemplified by an implementation on the KM4CCD system, a κ goniometer with CCD detector. It was tailored towards the requirements of this particular instrument. However, the expressions presented allow a straightforward extension towards more general instruments like goniometers with two-axis θ arms (goniometers for experimental phase determination). Furthermore, the model is also applicable to other diffraction geometries like Euler-cradle goniometers and fixed-axis machines (one-, two- and three-axis goniometers). If the imaging-detector component is ignored, the model may also be applied to conventional goniometers of any complexity.

The model has been successfully applied in the calibration of the KM4CCD system. The proposed reference-crystal calibration scheme allows the extraction of high-quality cell data from imaging diffractometers. The experimental and simulation data revealed that the uncertainty in extraction of diffraction angles and peak positions may impair both the unit-cell quality (lattice deformation) and the instrument model. A good instrument calibration can be obtained by using a high-symmetry standard crystal (cubic is preferred owing to its single-parameter orthonormalization matrix) along with reasonably narrow frame widths (0.25–1°). The calibration data set should include a variety of goniometer settings (at least 10–15) spanning isotropically the Ewald sphere. This data set can be used to optimize all relevant instrument parameters and can be used for subsequent experiments.

Another potential extension of the calibration procedure described here is the use of a separate experiment to obtain the geometric beam-detector relation: By measuring a powder pattern of a high-symmetry sample, additional observations for the highly correlated beam-detector relations may be obtained. Algorithms for fitting ellipse patterns are readily available (Pilu *et al.*, 1996).

Table 4. *Calibration of the KM4CCD system using three different wavelengths*

Reference crystal alum $KAl(SO_4)_2 \cdot 12H_2O$ (Larson & Cromer, 1967). Note that the instrument constants α_φ and α_κ, which are wavelength independent, reproduce within standard uncertainties The deviations of the lattice constants determined with Ag radiation can be attributed to the different bandpass (low monochromator glancing angle) of the graphite monochromator for this wavelength as compared to Cu and Mo.

Parameter	Cu	Mo	Ag
N^{obs}	604	1522	1111
N^{frames}	600	750	300
T^{exp} (s)	10	4	15
ω^{step} (°)	0.5	0.2	0.5
χ^2	0.014	0.014	0.019
Δ_ω (°)	0.13 (4)	−0.00 (2)	0.05 (3)
Δ_κ (°)	0.04 (3)	0.12 (2)	0.03 (1)
α_κ (°)	50.08 (3)	50.11 (2)	50.06 (3)
α_φ (°)	−0.04 (3)	0.05 (2)	−0.02 (3)
Δ_θ (°)	0.3 (2)	0.2 (1)	0.3 (1)
d_0 (mm)	71.58 (5)	71.55 (3)	71.51 (4)
X_0 (pixels)	520 (4)	517 (2)	520 (2)
Y_0 (pixels)	486 (4)	486 (2)	485 (2)
φ_x^d (°)	0.16 (4)	0.13 (2)	0.17 (2)
φ_y^d (°)	0.27 (2)	0.20 (1)	0.27 (1)
φ_y^s (°)	0.01 (5)	−0.04 (2)	−0.03 (2)
a^* (Å^{-1})	0.8221 (2)	0.8218 (2)	0.8207 (3)
a (Å)	12.164 (3)	12.164 (2)	12.185 (2)
b (Å)	12.167 (3)	12.165 (2)	12.185 (2)
c (Å)	12.166 (3)	12.173 (3)	12.182 (2)
α (°)	89.98 (2)	90.00 (1)	90.03 (1)
β (°)	89.98 (2)	90.03 (1)	90.01 (1)
γ (°)	89.98 (2)	90.01 (1)	90.02 (1)
V (Å^3)	1800.45	1801.33	1808.68

We would like to acknowledge the careful reading of one of the referees, which helped to clearify the article. The financial support of the Swiss National Science Foundation (grant No. 20-46666.96) is gratefully acknowledged.

References

Arndt, U. W. & Wonacott, A. J. (1977). Editors. *The Rotation Method in Crystallography*. Amsterdam: North Holland.

Bernal, J. D. (1923). Occasional Paper No. 1, Department of Crystallography, Birkbeck College, London (1981).

Bricogne, G. (1986). Proceedings of the ECC Cooperative Workshop on Position-Sensitive Detector Software (Phases I and II), LURE, 26 May–7 June 1986, pp. 109–111.

Busing, W. R. & Levy, H. A. (1967). *Acta Cryst.* **22**, 457–464.

Christensen, A. T. & Thom, E. (1971). *Acta Cryst.* B**27**, 581–586.

Diamond, R. (1990). *Proc. R. Soc. London Ser. A*, **428**, 451–472.

Golub, G. H. & Van Loan, C. F. (1996). *Matrix Computations*, 3rd ed. Johns Hopkins Studies in the Mathematical Sciences.

Kabsch, W. (1988). *J. Appl. Cryst.* **21**, 67–71.

Larson, A. C. & Cromer, D. T. (1967). *Acta Cryst.* **22**, 793–800.

Milch, J. R. & Minor, T. C. (1974). *J. Appl. Cryst.* **7**, 502–505.
Paciorek, W. A., Meyer, M. & Chapuis, G. (1999). *J. Appl. Cryst.* **32**, 11–14.
Pilu, M., Fitzgibbon, A. & Fisher, R. B. (1996). IEEE International Conference on Image Processing, Lausanne, September 1996.
Press, W. H., Teukolsky, S. A., Vetterling, W. T. & Flannery, B. P. (1994). *Numerical Recipes in C*, 2nd ed. Cambridge University Press.
Prince, E. (1994). *Mathematical Techniques in Crystallography and Materials Science*. Berlin: Springer-Verlag.
Spena, F. R. (1993). *Il Nuovo Cimento* **108**B, No. 6, 689–698.
Thomas, D. J. (1990). *Acta Cryst.* A**46,** 321–343.
Thomas, D. J. (1992). *Acta Cryst*. A**48**, 134–158.
Tucker, P. (1986). Proceedings of the ECC Cooperative Workshop on Position-Sensitive Detector Software (Phases I and II), LURE, 26 May–7 June 1986, pp. 49–56.
Wilkinson, C. (1990). *J. Appl. Cryst.* **23**, 111–114.